Atmos. Meas. Tech., 2, 337–353, 2009
www.atmos-meas-tech.net/2/337/2009/

Atmospheric Measurement Techniques

MIPAS reduced spectral resolution UTLS-1 mode measurements of temperature, O_3, HNO_3, N_2O, H_2O and relative humidity over ice: retrievals and comparison to MLS

S. Chauhan[1], M. Höpfner[1], G. P. Stiller[1], T. von Clarmann[1], B. Funke[2], N. Glatthor[1], U. Grabowski[1], A. Linden[1], S. Kellmann[1], M. Milz[1,*], T. Steck[1,], H. Fischer[1], L. Froidevaux[3], A. Lambert[3], M. L. Santee[3], M. Schwartz[3], W. G. Read[3], and N. J. Livesey[3]**

[1]Institut für Meteorologie und Klimaforschung, Forschungszentrum Karlsruhe, Karlsruhe, Germany
[2]Instituto de Astrofísica de Andalucía CSIC, Granada, Spain
[3]Jet Propulsion Laboratory, California Institute of Technology, Pasadena, California, USA
[*]now at: LuleåTekniska Universitet Institutionen för Rymdvetenskap, Kiruna, Sweden
[**]now at: Gymnasium, Neckartenzlingen, Germany

Received: 22 December 2008 – Published in Atmos. Meas. Tech. Discuss.: 25 February 2009
Revised: 2 July 2009 – Accepted: 9 July 2009 – Published: 21 July 2009

Abstract. During several periods since 2005 the Michelson Interferometer for Passive Atmospheric Sounding (MIPAS) on Envisat has performed observations dedicated to the region of the upper troposphere/lower stratosphere (UTLS). For the duration of November/December 2005 global distributions of temperature and several trace gases from MIPAS UTLS-1 mode measurements have been retrieved using the IMK/IAA (Institut für Meteorologie und Klimaforschung/Instituto de Astrofísica de Andalucía) scientific processor. In the UTLS region a vertical resolution of 3 km for temperaure, 3 to 4 km for H_2O, 2.5 to 3 km for O_3, 3.5 km for HNO_3 and 3.5 to 2.5 km for N_2O has been achieved. The retrieved temperature, H_2O, O_3, HNO_3, N_2O, and relative humidity over ice are intercompared with the Microwave Limb Sounder (MLS/Aura) v2.2 data in the pressure range 316 to 0.68 hPa, 316 to 0.68 hPa, 215 to 0.68 hPa, 215 to 3.16 hPa, 100 to 1 hPa and 316 to 10 hPa, respectively. In general, MIPAS and MLS temperatures are biased within ±4 K over the whole pressure and latitude range. Systematic, latitude-independent differences of −2 to −4 K (MIPAS-MLS) at 121 hPa are explained by previously observed biases in the MLS v2.2 temperature retrievals. Temperature differences of −4 K up to 12 K above 10.0 hPa are present both in MIPAS and MLS with respect to ECMWF (European Centre for Medium-Range Weather Forecasts) and are likely due to deficiencies of the ECMWF analysis data. MIPAS and MLS stratospheric volume mixing ratios (vmr) of H_2O are biased within ±1 ppmv, with indication of oscillations between 146 and 26 hPa in the MLS dataset. Tropical upper tropospheric values of relative humidity over ice measured by the two instruments differ by ±20% in the pressure range ∼146 to 68 hPa. These differences are mainly caused by the MLS temperature biases. Ozone mixing ratios agree within 0.5 ppmv (10 to 20%) between 68 and 14 hPa. At pressures smaller than 10 hPa, MIPAS O_3 vmr are higher than MLS by an average of 0.5 ppmv (10%). General agreement between MIPAS and MLS HNO_3 is within the range of −1.0 (−10%) to 1.0 ppbv (20%). MIPAS HNO_3 is 1.0 ppbv (10%) higher compared to MLS between 46 hPa and 10 hPa over the Northern Hemisphere. Over the tropics at 31.6 hPa MLS shows a low bias of more than 1 ppbv (>50%). In general, MIPAS and MLS N_2O vmr agree within 20 to 40 ppbv (20 to 40%). Differences in the range between 100 to 21 hPa are attributed to a known 20% positive bias in MIPAS N_2O data.

1 Introduction

Space-borne limb emission sounding is an established technique for monitoring the composition of the Earth's atmosphere above the middle troposphere. Its advantages are (1) high sensitivity to minor trace species, (2) good vertical resolution, (3) independence of sunlight, allowing the coverage of the whole Earth within one day. Currently five limb emission instruments are orbiting the Earth: Sub-Millimeter Radiometer (SMR) on Odin (Murtagh et al., 2002), HIRDLS (High Resolution Dynamics Limb Sounder) (Gille et al., 2008), TES (Tropospheric Emission Spectrom-

Correspondence to: S. Chauhan
(swarup.chauhan@imk.fzk.de)

eter) (Beer et al., 2001), MLS (Microwave Limb Sounder) (Waters et al., 2006) on the EOS (Earth Observing System) Aura and MIPAS (Michelson Interferometer for Passive Atmospheric Sounding) (Fischer et al., 2008) on the Envisat satellite. SMR and MLS are operating in the sub-millimeter and microwave spectral region, while HIRDLS, TES, and MIPAS are mid-infrared instruments. Of those, TES has the capability of limb and nadir sounding and is mainly operated in nadir mode. HIRDLS, MLS, SMR and MIPAS are operating exclusively in limb mode. Most studies using limb-emission data have concentrated on the stratosphere and higher atmosphere, but recently the applicability to the region of the UTLS has been demonstrated by e.g. Glatthor et al. (2007); Jiang et al. (2007); von Clarmann et al. (2007); Eriksson et al. (2007); Su et al. (2006); Wu et al. (2005); Read et al. (2004, 1995).

Ceccherini et al. (2008) showed studies on the quality of MIPAS low resolution O_3 data and comparison with co-located measurements by GOMOS (Global Ozone Monitoring by Occultation of Stars). The present work shows comparisons of co-located measurements between the common retrieval quantities of MLS v2.2 and MIPAS low resolution data. This is a prerequisite for a possible combination of complementary parameters between the two instruments (e.g. differing trace gases, the same trace gases obstructed by thin clouds in case of mid-IR or by water vapour in case of microwave observations). The emphasis is on the region of the upper troposphere to the middle stratosphere when MIPAS was operated in UTLS-1 mode.

2 MIPAS measurements and data processing

2.1 Instrument and observations

MIPAS (Fischer et al., 2008) is a Fourier transform spectrometer taking high-spectral-resolution limb observations of the Earth's radiation from 685 cm^{-1} to 2410 cm^{-1} (14.6–4.15 μm). It was launched on 1 March 2002 on the Environmental satellite Envisat by the European Space Agency (ESA). It is orbiting in a sun-synchronous polar orbit at 800 km altitude with an inclination of 98.55° and an ascending equatorial crossing time of 10:00. From July 2002 until March 2004, MIPAS took measurements with maximum optical path difference (OPD) of 20 cm corresponding to a 'high' spectral resolution of 0.025 cm^{-1}. During this time MIPAS measured mostly in its nominal mode, with a limb scan distance of ∼500 km and 17 tangent heights covering an altitude range from 7 to 69 km. MIPAS provides nearly full global (or pole-to-pole) coverage with a latitude range of 87° S to 87° N. Due to problems with the interferometer mirror slide system, MIPAS performed few operations from April–December 2004. In January 2005 regular observations resumed, but with reduced duty cycle and a reduced spectral resolution (RR) of 0.0625 cm^{-1} (OPD=8.0 cm). The reduced spectral resolution has the advantage that more spectra can be measured during the same time interval compared to the former "high" spectral resolution observations. Various dedicated observation modes are being operated (http://www.atm.ox.ac.uk/group/mipas/rrmodes.html), most performing vertical oversampling intended for better sampling of the UTLS region.

In UTLS-1 mode MIPAS measures at 19 tangent points; tangent altitudes are latitude-dependent from 7 to 50 km over the poles and 13 to 56 km over the equator. A latitude-dependent floating altitude-sampling grid is used in order to follow roughly the tropopause height along the orbit with the requirement to collect at least one spectrum within the troposphere but to avoid too many cloud-affected spectra. For the 2002–2003 operational period this approach had not been implemented for reasons of simplicity. The vertical sampling grid spacing between the tangent altitudes is 1.5 km from 8.5 to 22 km, 2.0 km from 22 to 28 km, 3.0 km from 28 to 34 km and 4.5 km from 34 to 52 km. Thus, compared to the 3 km vertical field-of-view extent of MIPAS, an oversampling of up to a factor of 2 is achieved up to 28 km. As will be shown below, this leads to an improved vertical resolution from 2 to 4 km in the UTLS region of the resulting trace gas profiles of RR UTLS-1 mode compared to the vertical resolution of 3 to 4 km in the full resolution (FR) nominal mode observations.

2.2 MIPAS IMK-IAA data processing

Retrievals for temperature (T) and line-of-sight (LOS) in terms of the tangent point altitude, H_2O, O_3, HNO_3 and N_2O in the RR UTLS-1 mode were performed using the IMK/IAA data processor (von Clarmann et al., 2003) on the basis of ESA version IPF 4.67 calibrated radiance spectra. For the FR mode observations, the retrieval approach and comparisons/validation have been described in the following publications: T/LOS: von Clarmann et al. (2003), Wang et al. (2005); H_2O: Milz et al. (2005); O_3: Steck et al. (2007); HNO_3: Wang et al. (2007); N_2O: Glatthor et al. (2005). MIPAS retrievals make use of narrow wavelength regions (so-called microwindows) (Echle et al., 2000). The microwindows which were used for the evaluation of the FR measurements have been adapted to the RR UTLS-1 mode (Table 1). Further, cloud contaminated spectra are removed using the method of Spang et al. (2004).

The retrieval of temperature and trace gas profiles is performed for most cases sequentially. First, the spectral shift of the measurement is determined. Second, temperature and elevation of the LOS of the instrument are jointly retrieved. Thereafter, H_2O, O_3, HNO_3 and CH_4 along with N_2O are computed (von Clarmann et al., 2009b).

The retrieval procedure itself follows the scheme described by Rodgers (2000):

$$\boldsymbol{x}_{i+1}=\boldsymbol{x}_i+(\mathbf{K}_i^T\mathbf{S}_y^{-1}\mathbf{K}_i+\mathbf{R})^{-1}\times\left[\mathbf{K}_i^T\mathbf{S}_y^{-1}(\boldsymbol{y}-\boldsymbol{f}(\boldsymbol{x}_i))-\mathbf{R}(\boldsymbol{x}_i-\boldsymbol{x}_a)\right]. \quad (1)$$

Here $\boldsymbol{x}$ is the retrieval vector, $\mathbf{K}$ is the Jacobian matrix containing the partial derivatives of the spectra with respect to the retrieval vector, $\mathbf{S}_y$ is the covariance matrix due to measurement noise, $\mathbf{R}$ is a regularization or constraint matrix, $\boldsymbol{y}$ is the measurement vector, $\boldsymbol{f}$ the forward model, $\boldsymbol{x}_a$ the a priori profile, and i the iteration index.

The atmospheric state is retrieved on a finer vertical retrieval grid (gridwidth 1 km up to 44 km, 2 km up to 70 km and 5 km above), compared to the tangent altitude grid spacing. To stabilise the retrievals, a Tikhonov smoothing constraint (Tikhonov, 1963) is applied where

$$R = \alpha \mathbf{L}_1^T \mathbf{L}_1. \quad (2)$$

Here, $\mathbf{L}_1$ is the first order derivative matrix (Steck, 2002). The regularization strength α has been adapted to obtain best possible vertical resolution in the UTLS region yet avoiding unstable retrievals.

The retrieval approach developed for the UTLS-1 mode parameters has been adopted as far as possible to the FR mode. The changes between the RR nominal mode (which are equivalent to those of the RR UTLS-1 mode) compared to FR mode are described in detail by von Clarmann et al. (2009b). In summary, the following adaptations have been made. (1) Microwindows: Table 1 lists the channels and the range of microwindows used for temperature/LOS and trace gases in the UTLS-1 mode retrieval setup. Spectral boundaries have been adjusted to suite the spectral resolution and sampling of the RR resolution UTLS-1 mode. Further, due to problems of spectral grid points affected by non-local thermodynamic equilibrium radiation, corresponding microwindows have been discarded. (2) Zero a priori profiles $\boldsymbol{x}_a$ for all trace gases in combination with (3) latitude and, as far as possible, altitude-independent regularization strengths are applied, such that the regularization results in a smoothing of the profiles without biasing them towards the a priori (von Clarmann et al., 2009b). (4) Horizontal temperature inhomogeneities as gradient profiles are taken into account during all the trace gas retrievals helping to improve on retrieval convergence. (5) In the case of H_2O, log(vmr) instead of vmr values are used as primary retrieval parameters. This helps in constraining the vmr profiles in spite of the large dynamic variation of H_2O in the upper troposphere.

2.3 Vertical resolution, horizontal resolution and error estimation

In this section we present a diagnosis of the MIPAS UTLS-1 retrievals in terms of resolution and error estimation.

The vertical resolution is determined from the averaging kernel matrix $\mathbf{A}$ of the retrieval (Rodgers, 2000):

$$\mathbf{A} = (\mathbf{K}_i^T \mathbf{S}_y^{-1} \mathbf{K}_i + \mathbf{R})^{-1} \mathbf{K}_i^T \mathbf{S}_y^{-1} \mathbf{K}_i. \quad (3)$$

The rows of the averaging kernel matrix give the contribution of the true values to the retrieved values, whereas its columns are responses with respect to delta-peak-like perturbations at each altitude. The estimated measurement noise error is obtained from the error covariance matrix (Rodgers, 2000):

$$\mathbf{S}_n = (\mathbf{K}^T \mathbf{S}_y^{-1} \mathbf{K} + \mathbf{R})^{-1} \mathbf{K}^T \mathbf{S}_y^{-1} \mathbf{K} (\mathbf{K}^T \mathbf{S}_y^{-1} \mathbf{K} + \mathbf{R})^{-1}. \quad (4)$$

For estimation of systematic errors $\Delta \boldsymbol{x}_b$ the linear mapping of the standard deviation σ_b of each uncertainty parameter b is used:

$$\Delta \boldsymbol{x}_b = (\mathbf{K}^T \mathbf{S}_y^{-1} \mathbf{K} + \mathbf{R})^{-1} \mathbf{K}^T \mathbf{S}_y^{-1} \mathbf{K}_b \sigma_b, \quad (5)$$

where $\mathbf{K}_b$ is the Jacobian of the measurement with respect to the uncertainty parameter b.

Figures 1 to 5 show the vertical resolution and the estimated measurement noise of temperature, H_2O, O_3, HNO_3 and N_2O distributions along one orbit in RR UTLS-1 mode (orbit 19595; 28–29 November 2005), compared with those of the FR nominal mode (orbit 09017; 21 November 2003). Up to ∼30 km in the RR UTLS-1 mode, temperature and trace gas profiles have a vertical resolution of 2 to ∼4 km due to vertical oversampling, degrading to ≥5 km further up due to the larger tangent point distance. In the case of FR nominal mode the vertical resolution is 3.5 to ∼5 km up to ∼40 km. The latitudinal wave-like pattern of the vertical resolution and estimated measurement noise in case of the RR UTLS-1 mode is caused by its latitude-dependent tangent altitude grid as described above. In comparison, such a structure does not appear in the figures for the FR nominal mode since there the tangent altitudes were fixed with latitude. The strong variations of the vertical resolution with altitude, clearly visible above 30 km in case of UTLS-1 mode and from 10 km to 50 km in case of FR nominal mode is caused by the finer spacing of the retrieval levels compared to the tangent altitude grid. Typically at retrieval altitudes close to a tangent altitude the resolution is better than in between.

Table 1. Microwindows selected for MIPAS low resolution data for UTLS 1 mode.

Gases	MIPAS Bands used[a]	Microwindows in the range (cm^{-1})[b]
temperature	A(685–970)	(731.25–812.56)
H_2O	A(685–970), B(1215–1500), C(1570–1750)	(795.75–1603.43)
O_3	A(685–970), AB (1020–1170)	(760.69–1039.00)
HNO_3	A(685–970)	(862.50–883.62)
N_2O	B(1215–1500)	(1227.81–1303.12)

[a] A, B, C and AB are the spectral band of MIPAS used for RR UTLS-1 mode measurement.
[b] These are the paticular spectral regions selected from bands given in column 2 for specific analysis.

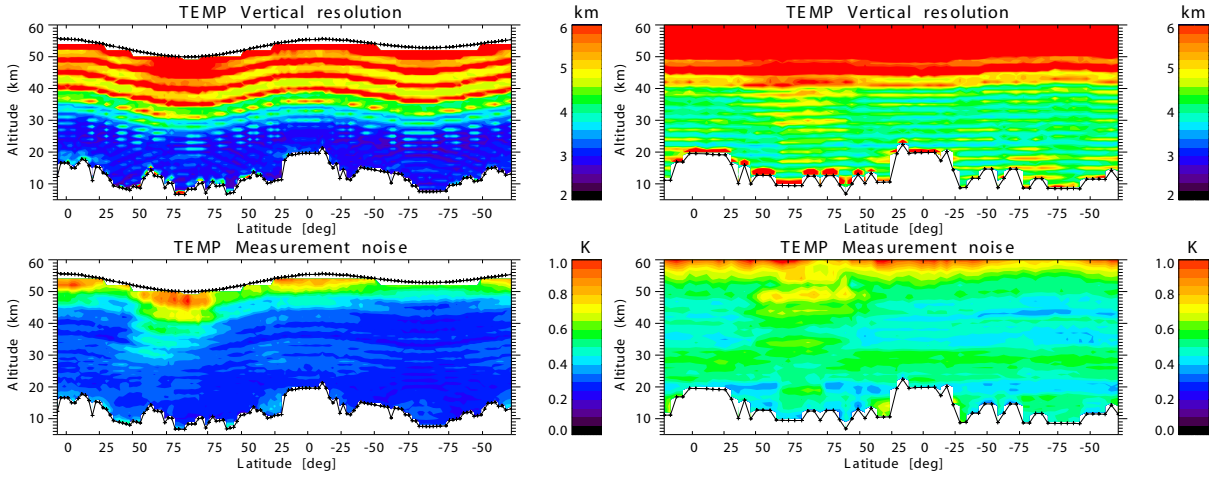

Fig. 1. Vertical resolution of temperature on 28–29 November 2005 obtained from one single orbit 19595 in MIPAS RR UTLS-1 mode (upper left) and for 21 November 2003 from orbit 09017 in FR mode (upper right). Corresponding retrieved measurement noise in RR UTLS-1 mode (lower left) and FR mode (lower right).

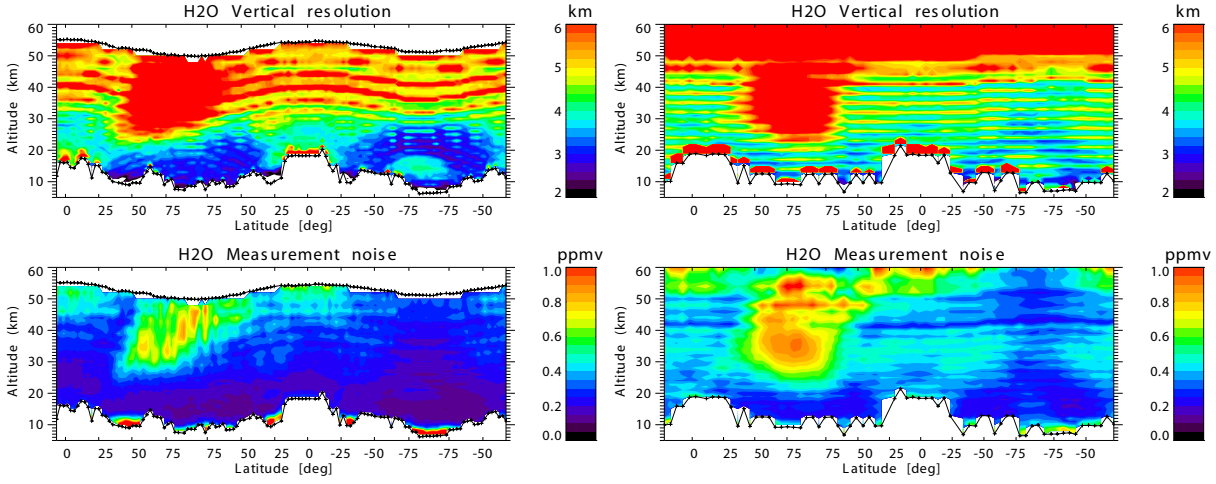

Fig. 2. Vertical resolution of H_2O on 28–29 November 2005 obtained from one single orbit 19595 in MIPAS RR UTLS-1 mode (upper left) and for 21 November 2003 from orbit 09017 in FR mode (upper right). Corresponding retrieved measurement noise in RR UTLS-1 mode (lower left) and FR mode (lower right).

Vertical resolution is defined as the column FWHM (full-width half-maximum). The estimated measurement noise is 0.2–0.3 K for temperature, 0.1–0.3 ppmv for H_2O, 0.03–0.09 ppmv for O_3, ~0.05 ppbv for HNO_3 and 4.0 ppbv for N_2O up to a height of 30 km in RR UTLS-1 mode. In the case of full resolution nominal mode the absolute noise error is generally higher than RR UTLS-1 mode (Figs. 1 to 5). The change in the vertical resolution and the estimated measurement noise with latitude (observed more prominently in the case of H_2O) is due to the MIPAS sensitivity to temperatures and the height constant regularization used. Because it is summer in the Southern Hemisphere during November–December, relatively better signal to noise ratio is observed compared to that in the Northern Hemisphere, accounting for latitudinal variation in the vertical resolution and estimated measurement noise.

Horizontal averaging kernels were derived in order to characterize the smoothing caused by the assumption of horizontal homogeneity in the limb observations (von Clarmann et al., 2008). We report (Table 2) the horizontal resolution of temperature and trace gases for a reference geolocation over the southern polar region (orbit 19306; 8 November 2005), in terms of full width at half maximum (FWHM) of the rows of the averaging kernel matrix (Rodgers, 2000; von Clarmann et al., 2009a). Variations in the horizontal resolution with altitude are due to the fact that the in the regularized retrieval

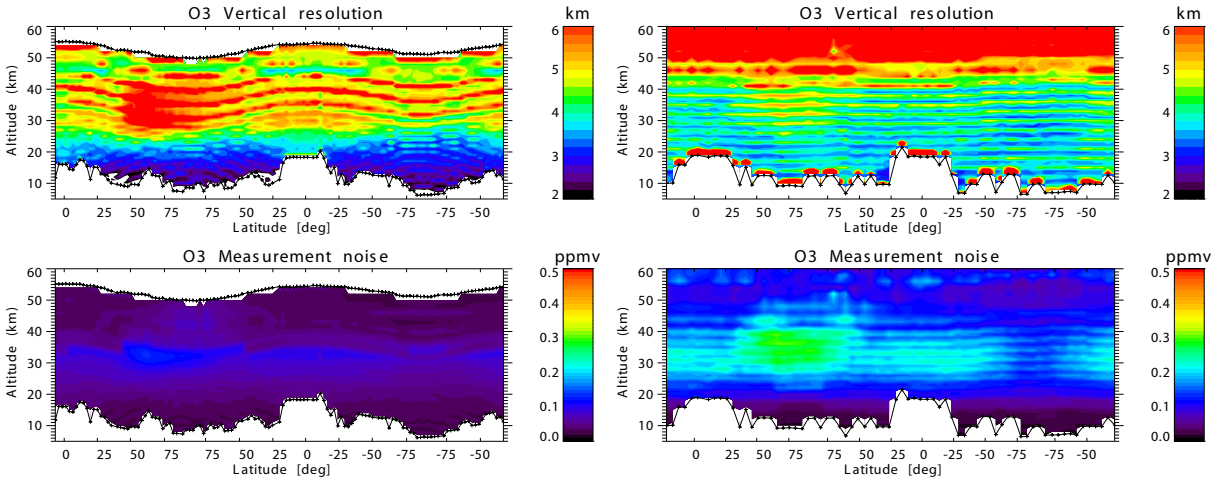

Fig. 3. Vertical resolution of O_3 on 28–29 November 2005 obtained from one single orbit 19595 in MIPAS RR UTLS-1 mode (upper left) and for 21 November 2003 from orbit 09017 in FR mode (upper right). Corresponding retrieved measurement noise in RR UTLS-1 mode (lower left) and FR mode (lower right).

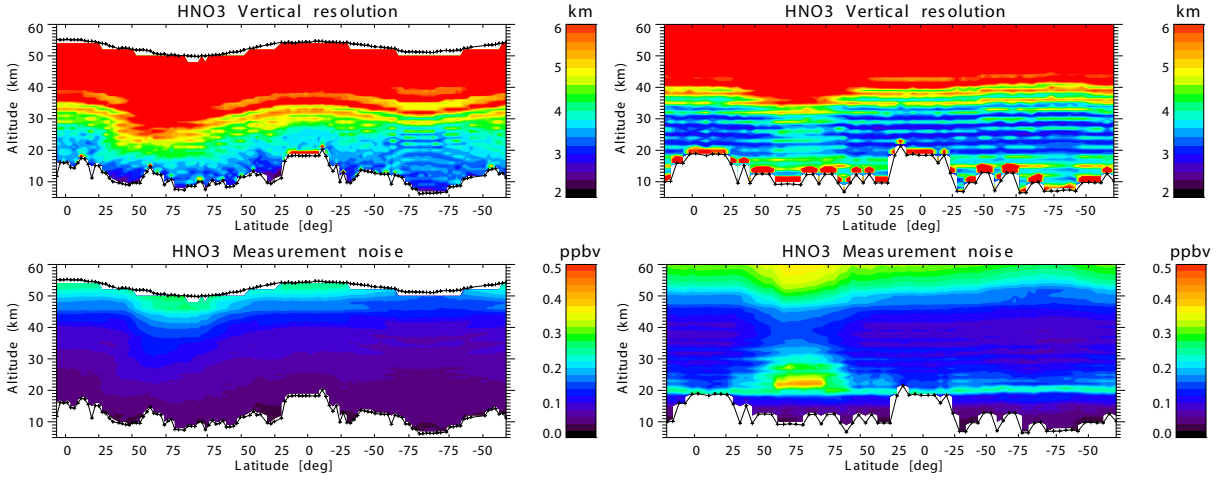

Fig. 4. Vertical resolution of HNO_3 on 28–29 November 2005 obtained from one single orbit 19595 in MIPAS RR UTLS-1 mode (upper left) and for 21 November 2003 from orbit 09017 in FR mode (upper right). Corresponding retrieved measurement noise in RR UTLS-1 mode (lower left) and FR mode (lower right).

horizontal smearing is coupled with vertical resolution and, thus, is subjected to similar variations. The values of horizontal resolution given here are intended as an exemplary case. There will be differences depending on the actual state of the atmosphere.

Table 3a–e give results of the linear error analysis for temperature and trace gases calculated on the basis of a reference limb scan over mid-latitudes (7 November 2005; 01:35 UT). The total error is calculated as the quadratic combination of measurement noise error and parameter errors due to uncertainties in interfering gases, temperature, temperature gradient, LOS, spectral shift, gain calibration and instrument line shape. In the case of temperature the total error is dominated by the parameter error. In the case of H_2O, O_3, HNO_3 and N_2O the parameter error is the main contributor to the

Table 2. Horizontal resolution in terms of full width at half maximum of the rows of the horizontal averaging kernels.

Single scan of orbit 19306 on 8 November 2005 over the southern polar latitudes

Altitude (km)	T (km)	H_2O (km)	O_3 (km)	HNO_3 (km)	N_2O (km)
10	173	146	317	209	97
15	113	210	155	280	241
20	197	122	347	321	226
30	102	117	365	150	107
40	170	111	200	119	183
50	111	76	431	77	83

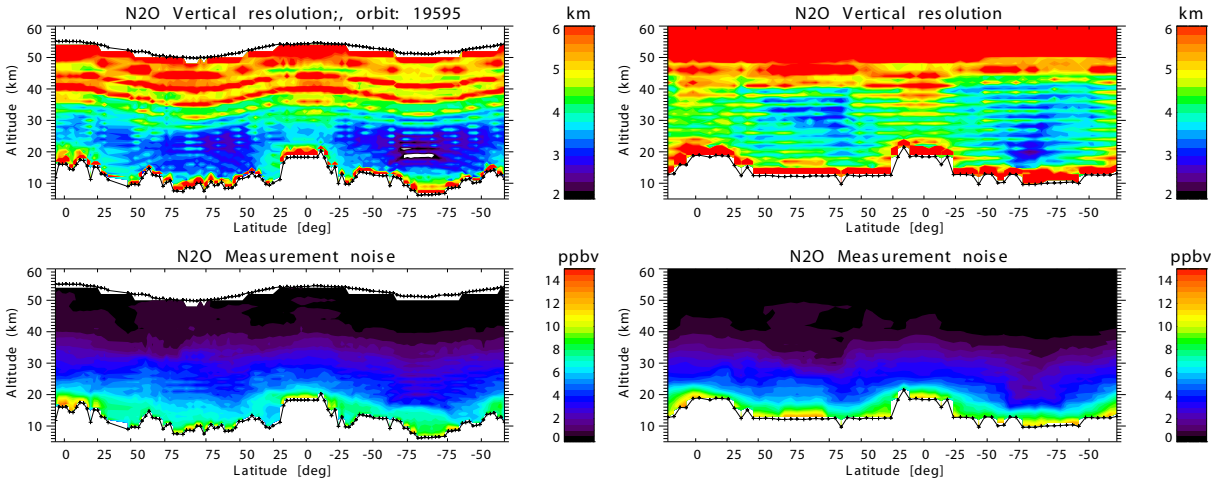

Fig. 5. Vertical resolution of N_2O on 28–29 November 2005 obtained from one single orbit 19595 in MIPAS RR UTLS-1 mode (upper left) and for 21 November 2003 from orbit 09017 in FR mode (upper right). Corresponding retrieved measurement noise in RR UTLS-1 mode (lower left) and FR mode (lower right).

Table 3a. Error budget determined for a single scan of orbit 19281 on 7 November 2005 in the northern mid-latitudes for selected altitudes.

Temperature			
Altitude (km)	Total error[a]	Measurement noise	Parameter error[b]
10	3.4	0.32	3.4
15	1.2	0.27	1.1
20	0.59	0.28	0.52
30	0.59	0.31	0.51
40	0.92	0.45	0.81
50	1.5	0.88	1.2

[a] Total errors are the quadratic combination of measurement noise and parameter error and are given in K.
[b] Parameter error is the quadratic combination of error contributions from interfering gases which are not jointly fitted, and from spectral shift, gain calibration and instrumental line-shape uncertainties.

total error up to 30 km, and LOS and temperature uncertainty are the dominant contributors to the parameter error in this height range. Above 30 up to 50 km measurement noise contributes significantly to the total error.

Table 3b. Continued.

H_2O					
Altitude (km)	Total error[a]	Measurement noise	Parameter error[b]	Line-of-sight (LOS)[c]	Temp.[d]
10	5.1(32)	0.57(4)	5(31)	4.8(31)	1.1(7)
15	0.35(7)	0.16(3)	0.32(7)	0.28(6)	0.08(2)
20	0.26(6)	0.15(3)	0.21(5)	0.19(4)	0.05(1)
30	0.43(8)	0.31(6)	0.3(6)	0.19(3)	0.16(3)
40	0.75(11)	0.67(9)	0.34(5)	0.06(1)	0.02(<1)
50	0.86(23)	0.57(15)	0.64(15)	0.03(3)	0.2(3)

[a] Total errors are the quadratic combination of measurement noise and parameter error. Absolute values of the total error are in ppmv and relative values are given in parentheses (%).
[b] Parameter error is the quadratic combination of error contributions from interfering gases which are not jointly fitted, and from temperature, temperature gradient, LOS (in terms of tangent point altitude), spectral shift, gain calibration and instrumental line-shape uncertainties.
[c] Based on tangent altitude uncertainty of 150 m. LOS uncertainties contribute to the parameter errors but are given explicitly because of their dominant role.
[d] Based on temperature uncertainty of 1 K. Temperature uncertainties contribute to the parameter errors but are given explicitly because of their dominant role.

3 MLS instrument and data

Aura MLS was launched on 15 July 2004 into a near polar sun-synchronous orbit at 705 km altitude, with ascending equatorial crossing time of 13:45 (Schoeberl et al., 2006). It scans the Earth's limb providing 240 scans per orbit, spaced ∼165 km along the orbit track, and ∼3500 vertical profiles per day, with near pole-to-pole global latitudinal coverage from 82° S to 82° N.

The MLS data processing algorithm is based on the optimal estimation method and uses a two-dimensional retrieval approach to determine temperature, geo-potential height and trace gas concentrations (Livesey et al., 2006). Most data products are retrieved on a fixed vertical pressure grid with 6 levels per decade change in pressure from the troposphere to the stratosphere. In case of temperature and H_2O, the vertical pressure grid is finer in the troposphere and the lower stratosphere, with 12 levels per decade change in pressure

Table 3c. Continued.

O_3					
Altitude (km)	Total error[a]	Measurement noise	Parameter error[b]	LOS[c]	Temp.[d]
10	0.04(114)	0.04(105)	0.02(41)	0(26)	0(15)
15	0.05(7)	0.03(5)	0.04(6)	0.04(5)	0.01(1.5)
20	0.10(4)	0.04(2)	0.09(3)	0.04(1)	0.01(<1)
30	0.35(5)	0.09(1)	0.34(5)	0.25(4)	0.11(2)
40	0.43(7)	0.07(1)	0.43(7)	0.22(4)	0.25(4)
50	0.23(5)	0.05(4)	0.22(3)	0.11(2)	0.07(<1)

[a] Total errors are the quadratic combination of measurement noise and parameter error. Absolute values of the total error are in ppmv and relative values are given in parentheses (%).
[b] Parameter error is the quadratic combination of error contributions from interfering gases which are not jointly fitted, and from temperature, temperature gradient, LOS (in terms of tangent point altitude), spectral shift, gain calibration, and instrumental line-shape uncertainties.
[c] Based on tangent altitude uncertainty of 150 m. LOS uncertainties contribute to the parameter errors but are given explicitly because of their dominant role.
[d] Based on temperature uncertainty of 1 K. Temperature uncertainties contribute to the parameter errors but are given explicitly because of their dominant role.

between 1000 and 22 hPa (0–25 km). For this study MLS version 2.2 (v2.2) data (Livesey et al., 2006) have been used.

The vertical resolution of MLS data products has been reported as follows. Temperature: 6–3 km from 316–31.4 hPa, degrading to ∼4 km up to 1 hPa (Schwartz et al., 2008). H_2O: 1.5–4 km from 316 to 1 hPa (Read et al., 2007; Lambert et al., 2007). O_3: 2.5–3 km from 215–1 hPa (Livesey et al., 2006; Froidevaux et al., 2008). HNO_3: 3–5 km from 215–3.2 hPa (Santee et al., 2007). N_2O: 4–6 km from 100–4.6 hPa (Lambert et al., 2007).

Some findings reported in MLS validation papers which are relevant for the further discussion are: pressure-depedent temperature biases between 316 and 10 hPa (Schwartz et al., 2008), vertical oscillations in H_2O by up to 8% at 31.6 hPa (Read et al., 2007; Lambert et al., 2007), a small positive bias in O_3 at 22 hPa (Livesey et al., 2006; Froidevaux et al., 2008) and in HNO_3 a bias of ±5 to 15% throughout the stratosphere and ±30% at 215 hPa Santee et al. (2007).

4 Comparisons

MIPAS RR UTLS-1 mode data and MLS v2.2 data for the period of November–December 2005 are used for comparisons. A coincidence criterion of ±12 h in time and ±300 km in space was used to find matched profiles between MIPAS and MLS. This gave ∼300 to 350 coincident profiles over the poles/mid-latitudes and ∼50 to 250 matches over the sub-tropics and tropics. For MLS data, screening was done as specified in MLS v2.2 data quality document (http://mls.jpl.nasa.gov/data/datadocs.php). Since MIPAS and MLS have comparable vertical resolutions of ∼2 to 4 km in the region of the lower stratosphere, the profiles were compared directly without averaging kernel convolution (Rodgers, 2000).

Table 3d. Continued.

HNO_3					
Altitude (km)	Total error[a]	Measurement noise	Parameter error[b]	LOS[c]	Temp.[d]
10	0.06(11)	0.04(7)	0.05(8)	0.05(8)	0.01(2)
15	0.12(5)	0.05(2)	0.11(4)	0.09(3)	0.01(<1)
20	0.24(3)	0.06(<1)	0.24(3)	0.11(1)	0.05(<1)
30	0.37(5)	0.09(1)	0.36(5)	0.33(5)	0.09(1)
40	0.16(27)	0.14(24)	0.06(10)	0.05(8)	0(<1)
50	0.29(163)	0.26(153)	0.12(63)	0.03(20)	0.04(20)

[a] Total errors are the quadratic combination of measurement noise and parameter error. Absolute values of the total error are in ppbv and relative values are given in parentheses (%).
[b] Parameter error is the quadratic combination of error contributions from interfering gases which are not jointly fitted, and from temperature, temperature, LOS (in terms of tangent point altitude), spectral shift, gain calibration and instrumental line-shape uncertainties.
[c] Based on tangent altitude uncertainty of 150 m. LOS uncertainties contribute to the parameter errors but are given explicitly because of their dominant role.
[d] Based on temperature uncertainty of 1 K. Temperature uncertainties contribute to the parameter errors but are given explicitly because of their dominant role.

Table 3e. Continued.

N_2O					
Altitude (km)	Total error[a]	Measurement noise	Parameter error[b]	LOS[c]	Temp.[d]
10	20(6)	8.9(3)	18(5)	17(5)	0.25(<1)
15	17(5)	6.1(2)	15(5)	10(3)	9.7(3)
20	15(9)	4.8(2)	14(8)	13(7)	4.8(4)
30	7.5(9)	3.1(3)	6.9(8)	5.3(6)	3.5(4)
40	2.6(13)	1.6(8)	2.1(10)	0.5(3)	0.2(2)
50	1(83)	0.6(52)	0.8(61)	0.05(7)	0.2(18)

[a] Total errors are the quadratic combination of measurement noise and parameter error. Absolute values of the total error are in ppbv and relative values are given in parentheses (%).
[b] Parameter error is the quadratic combination of error contributions from interfering gases which are not jointly fitted, and from temperature, temperature gradient, LOS (in terms of tangent point altitude), spectral shift, gain calibration and instrumental line-shape uncertianties.
[c] Based on tangent altitude uncertainty of 150 m. LOS uncertainties contribute to the parameter errors but are given explicitly because of their dominant role.
[d] Based on temperature uncertainty of 1 K. Temperature uncertainties contribute to the parameter errors but are given explicitly because of their dominant role.

To assess the validity of the comparison between the two instruments in the upper troposphere it is necessary to understand the influence of the a priori there. Since in case of MIPAS a Tikhonov-type (Tikhonov, 1963) formalism with a smoothing constraint is applied, a strong a-priori weighting would lead to a smoothing of the profile of the retrieved atmospheric parameter but not to any systematic bias. In the case of MLS, the choice has been to minimize the influence of the a priori by using relatively loose constraints. In case of MIPAS we can directly evaluate a priori influence in the troposphere by analysing each individual averaging kernel matrix. These are not available in case of MLS. However, in the MLS data product values are flagged where retrieved precision worse than 50% of the a priori precision indicates a large weight of the a priori information in the result. Such values were rejected from the comparison. For co-incident data points of MIPAS and MLS in the upper troposphere we have calculated the mean vertical resolution of MIPAS from the averaging kernel. This resulted in values of about 3 km for temperature, 2.5 km for H_2O, 2.2 km for O_3 and 2.6 km for HNO_3 in comparison to MLS values of 5 km (T), 1.5–3.5 km (H_2O), 3 km (O_3) and 3.5 km (HNO_3), as given in literature for altitudes below 100 hPa (Schwartz et al., 2008; Livesey et al., 2008; Read et al., 2007; Santee et al., 2007). N_2O is not considered here because no significant number of tropospheric co-incidences has been found. Thus, in the upper troposphere, for the trace gases a direct comparison of the profiles from both instruments seems justified, while in case of temperature differences might be influenced by the differing vertical resolutions.

For the difference plots, first MIPAS altitude profiles of temperature and trace gases have been interpolated to the MLS pressure grid. Then for each pressure level the mean difference (MIPAS-MLS) of coincident profiles was calculated for each 5° latitude bin. These differences were plotted within the common pressure ranges of MLS and MIPAS as denoted by the black lines at the bottom and top in the difference plots. We note that in these figures the colour contours are interpolated linearly in latitude between the values centred at the mid-point of each latitude bin. The percentage differences and the bias between MIPAS and MLS are calculated as suggested by von Clarmann (2006).

The bias is determined from the equation:

$$b_j = \frac{1}{N_j} \sum_{i=1}^{N_j} \left[x_{ij}^{\mathrm{MIPAS}} - x_{ij}^{\mathrm{MLS}} \right] \tag{6}$$

where b_j and N_j are the bias and total number of coincident geolocations at j-th pressure level of MLS. $x_{ij}^{\mathrm{MIPAS}} - x_{ij}^{\mathrm{MLS}}$ are the difference values obtained from MIPAS and MLS i-th coincident profile pairs, at the j-th pressure level of MLS.

Percentage differences are determined with respect to mean MLS values:

$$b_j^{\mathrm{perc}} = \frac{b_j N_j}{\sum_{i=1}^{N_j} x_{ij}^{\mathrm{MLS}}} \times 100. \tag{7}$$

The uncertainty of the bias is reported in terms of the standard error of the mean (SEM), assuming independent differences:

$$\mathrm{SEM}_j = \frac{\sigma_j}{\sqrt{N_j}} \tag{8}$$

where σ_j is the standard deviation of the bias:

$$\sigma_j = \sqrt{\frac{\sum_{i=1}^{N_j} \left[x_{ij}^{\mathrm{MIPAS}} - x_{ij}^{\mathrm{MLS}} - b_j \right]^2}{(N_j - 1)}}. \tag{9}$$

4.1 Temperature

MIPAS and MLS temperature fields from November to December 2005 and their difference along with differences w.r.t ECMWF are shown in Fig. 6. Vertical oscillations typically up to ±4 K are observed between MIPAS and MLS in the pressure/latitude range from 316.2 to 100.0 hPa and ∼90° S to 90° N, respectively. MIPAS is colder by up to 1 K than MLS at the 21.5 hPa pressure level. In the middle and upper stratosphere MIPAS and MLS are biased within ±3 K. Differences up to ±4 K in the UTLS and in the stratosphere are in agreement with the differences observed in MLS in comparison to other satellite instruments (Schwartz et al., 2008).

Differences (MIPAS-ECMWF) and (MLS-ECMWF) are interpolated on to the MLS pressure grid. The agreement of MIPAS with ECMWF is within ±1.5 K while MLS temperatures show vertical oscillations of ±3 K w.r.t ECMWF analysis below 10.0 hPa. Above 10.0 hPa poor agreement is seen between MIPAS and ECMWF with differences of −4 K up to ≤12 K. MLS also shows similar poor agreement w.r.t ECMWF especially over the poles. Since the latitude dependence and magnitude of these differences w.r.t ECMWF are similar in case of MLS and MIPAS, they are probably due to errors in the ECMWF analysis dataset.

Figure 7 shows the global mean altitude-dependent bias between MIPAS and MLS together with the quadratically combined systematic and noise error estimates (1-σ), and the standard deviation of the differences between all matched profiles. The altitude-dependent mean bias varies between ±2.5 K peak-to-peak and lies within the combined systematic errors over the complete pressure range 316–0.1 hPa with small exceptions at 14.6 and 3.2 hPa. The combined random error varies by ±0.5–1 K and is by a factor of 3–5 smaller than the standard deviation of the differences. Thus, the estimated noise error does not account for the variability of the profiles. Possible reasons might be (1) the atmospheric variability, (2) an underestimation of the spectral noise error, or (3) a parameter error term which has been attributed to the systematic error budget, but which might also include random components. Given the magnitude of the systematic error term as plotted in Fig. 7 there could easily be a component which, when included in the estimated random error would

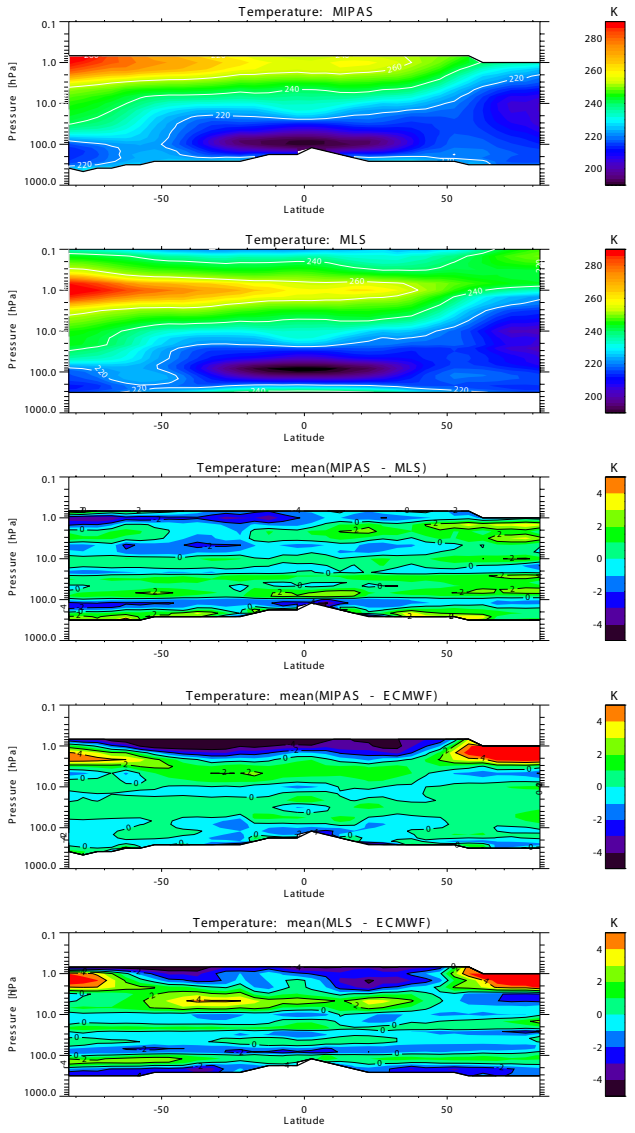

Fig. 6. Global temperature field from MIPAS and MLS and global mean differences for MIPAS-MLS, MIPAS-ECMWF, MLS-ECMWF from 6 November to 7 December 2005. Dark red and black colours represent values greater than +5 K and smaller than −4 K, respectively.

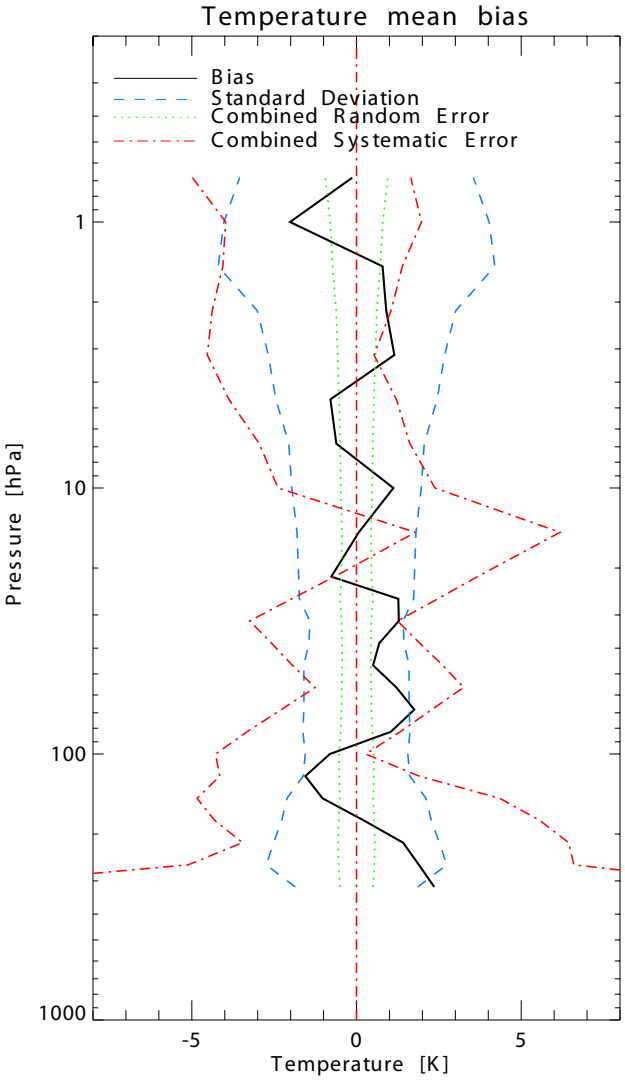

Fig. 7. Altitude-dependent global mean bias (MIPAS-MLS) and associated uncertainties from 6 November to 7 December 2005. The global mean bias is shown in black (thick line), the combined estimated measurement noise (1σ) in green (dotted), the combined systematic error (1σ) in red (dot-dashed) and the standard deviation of the differences in blue (dashed). The combinded systematic error is given asymmetric around zero as reported in Schwartz et al. (2008).

bring those in better agreement with the standard deviation, albeit not reducing the systematic errors strongly.

4.2 H_2O

In Figs. 8 and 9 global 2-D distributions of MIPAS and MLS H_2O, and their zonal differences are shown. Between 316.2 to 177.8 hPa (Fig. 9) over the mid-latitudes and poles MIPAS is wetter compared to MLS by about 50% (up to 100%), more prominently over the Southern Hemisphere. From 215.4 to 177.8 hPa over the sub-tropics and tropics MIPAS H_2O vmr's are drier by ∼10% compared to MLS.

Our MIPAS/MLS comparison, in the lower stratosphere (146.7–56.2 hPa; Fig. 8) shows oscillations of ±1 ppmv (±10%), over all latitudes. This "band" of oscillating values is seen to vary in altitude at different latitudes. Oscillations up to 10% are observed between 31.6–26.1 hPa for all latitudes. In the middle and upper stratosphere between 26.1–0.2 hPa the agreement between MIPAS and MLS is within ±5%.

Read et al. (2007), have also observed AIRS to be consistently wetter in comparison to MLS over the high latitudes in

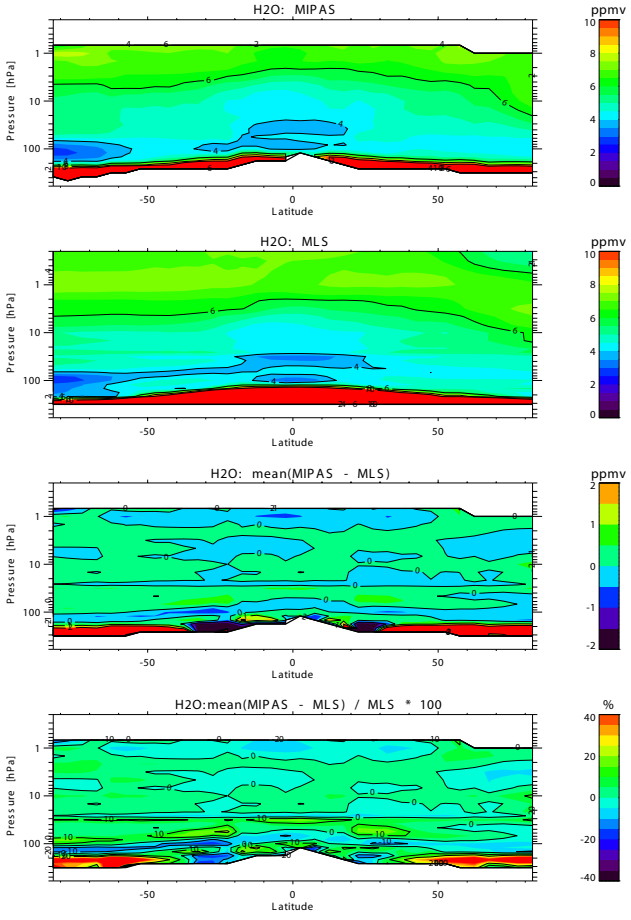

Fig. 8. Global H_2O fields of MIPAS and MLS from 6 November to 7 December 2005 together with mean absolute and relative differences. Colours beyond the colour scale (dark red and black) represent values outside the range of colour legend.

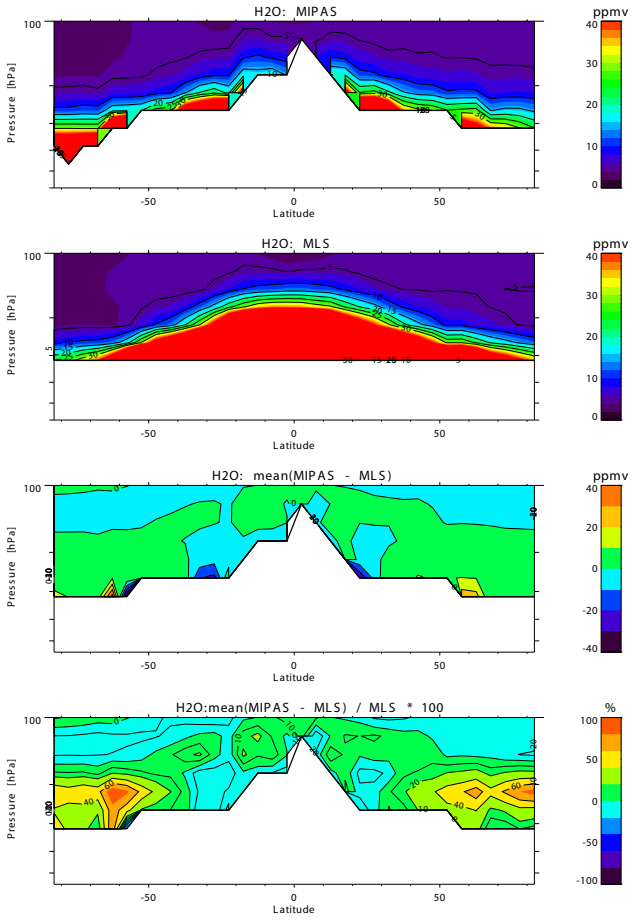

Fig. 9. Same as Fig. 8 but for UT.

the pressure range 316 to 178 hPa. The oscillations observed in the height range 31.6 to 26.1 hPa are due to a known artefact in MLS H_2O v2.2 retrievals (Lambert et al., 2007).

Figure 10 compares the global altitude-dependent mean bias and the standard deviation of its distribution with the estimated error budget. The altitude-dependent global mean bias is typically within ± 0.2 ppmv ($\pm 4\%$) between 100 to 0.1 hPa, with an exception at 31.6 hPa and 26.1 hPa were it varies from +0.4 (10%) to -0.2 (-4%) and, at 31.6 hPa, exceeds slightly the combined systematic error due to the problem in the MLS data as mentioned above (Read et al., 2007; Lambert et al., 2007). From 316 hPa to 100 hPa the mean bias varies from 12% to -4% within the systematic error estimates. Above about 100 hPa the standard deviation is only slightly higher than the estimated noise error. However, below this altitude the variability is much larger than estimated, most probably due to the strong natural atmospheric variability of water vapour at these altitudes.

A further factor which might contribute to the observed high variability in the upper troposphere might be the presence of cloud. In the ideal case that both measurements were performed at the same time and location there would be no difficulty because on basis of the MIPAS IR observations, cloud-affected altitudes are discarded from the comparison using a conservative cloud-detection scheme. In reality, beside different locations, there is a difference in time: MIPAS measures at around 10 and MLS at 01:40 local time. Thus, though for comparing two H_2O profiles, the conservative cloud free altitudes of MIPAS are used, there might be a cloud in the MLS field-of-view even at those heights. At that altitude this could either lead to higher water vapour in case of MLS compared to MIPAS because inside the cloud the humidity might be higher. On the other hand, cases can exist where MIPAS observes a cloud-free but supersaturated environment which is no more the case when there is a cloud present. We have tried to investigate the presence of such effects by subdividing the H_2O-comparisons into two sets. The first set contains only matches of daytime observations when there might be more clouds present in the early afternoon (when MLS measures) compared to morning observations

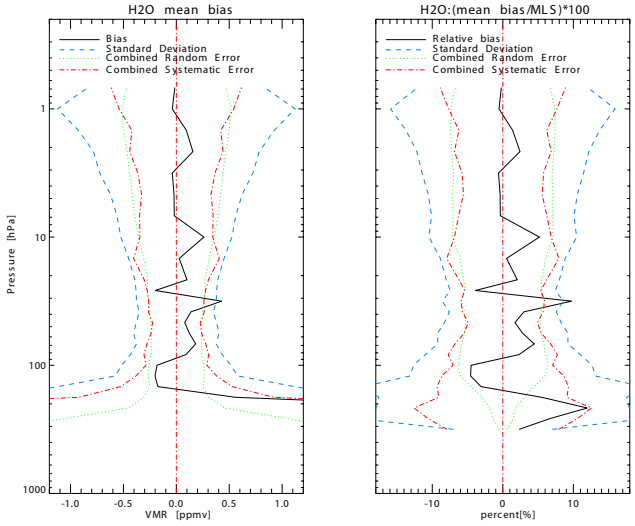

Fig. 10. Altitude-dependent global mean bias (MIPAS-MLS) (left panel), relative mean bias with respect to MLS (right panel) and over plotted associated uncertainties from 6 November to 7 December 2005 are shown. The global mean bias is shown in black (thick line), the combined estimated measurement noise (1σ) in green (dotted), the combined systematic error (1σ) in red (dot-dashed) and the standard deviation of the differences in blue (dashed).

by MIPAS. The second set consists of only nighttime data when the effect of clouds might be different. The results indicate a slightly larger dry bias of MIPAS compared to MLS in the region of the southern sub-tropical upper troposphere during day than during night. This is, however, not the case at the northern sub-tropics. In summary, we could not clearly identify a consistent picture pointing towards strong effects of clouds within the presented comparison. However, a contribution by cloud to the observed variability cannot be excluded.

4.3 Relative humidity over ice

Comparisons of tropical upper tropospheric relative humidity over ice (RHi) between MIPAS and MLS are shown in Fig. 11. MIPAS RHi profiles are computed using the formula by Goff and Gratch (1946) from MIPAS temperature and H_2O profiles. Over the tropics RHi up to 0.8–1 between 121.1 to 100.0 hPa are observed by MIPAS. In the case of MLS, RHi values of 0.8–1 are observed between 316.2 to 82.5 hPa and RHi>1 are observed from 68.1 up to 56.2 hPa. MIPAS/MLS (Fig. 11) differences of $\pm$0.2 are observed between 146.7 to 68.1 hPa. For further investigations two sets of RHi profiles were computed: (1) using MIPAS temperature and MLS H_2O, and (2) using MLS temperature and MIPAS H_2O. The difference MIPAS-set(1) showed a good agreement of 0 up to 0.1 (Fig. 12, top), while the difference MIPAS-set(2) (Fig. 12, bottom), showed large differences that were similar to those in the original comparison (Fig. 11). These Large differences between MLS and MIPAS mostly arise from the differences in the temperatures retrieved by the two instruments.

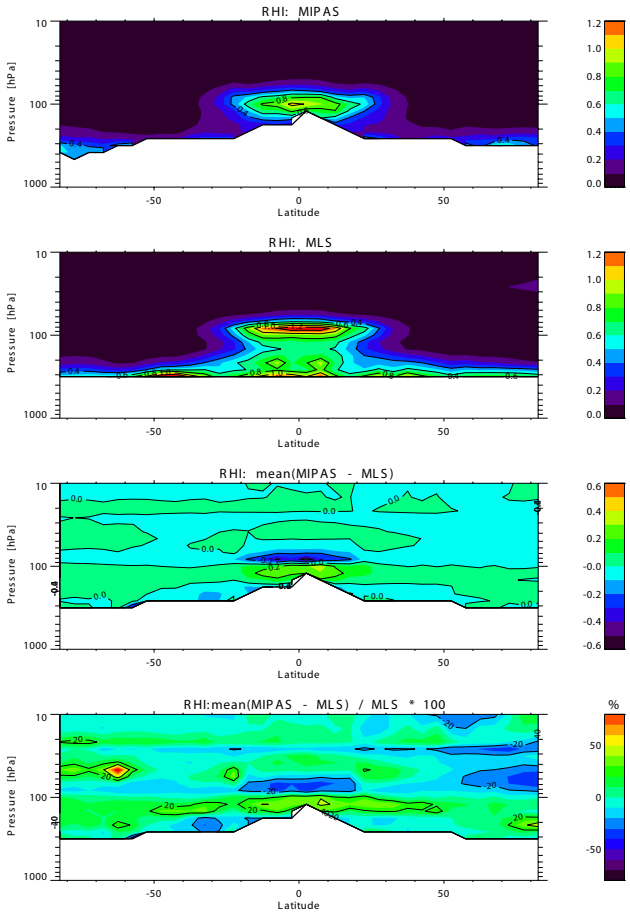

Fig. 11. Global RHi field of MIPAS and MLS from 6 November to 7 December 2005 together with their absolute and relative differences.

4.4 O_3

MIPAS and MLS O_3 zonal distributions and related differences are shown in Figs. 13 and 14. In the upper stratosphere (6.8–1.4 hPa) over the southern mid-latitudes and subtropics, MIPAS shows up to 10% higher values in comparison to MLS. Over the tropics at 31.6 hPa a difference (MIPAS-MLS) of 0.5 ppmv ($\sim$20%) is observed. Over the tropics and sub-tropics above the tropical tropopause layer (TTL) (100.0–68.1 hPa; Fig. 14) relative differences from $\sim$90% to $-$80% are observed. Over the south pole in the height range 146.7 to 100.0 hPa differences up to 10% are observed.

A comparison of MLS O_3 profiles with MIPAS RR nominal mode observations has been published by Froidevaux et al. (2008). They observed differences up to 10% in the upper stratosphere which agrees with our analysis of the MIPAS RR UTLS-1 mode here. Froidevaux et al. (2008) also report

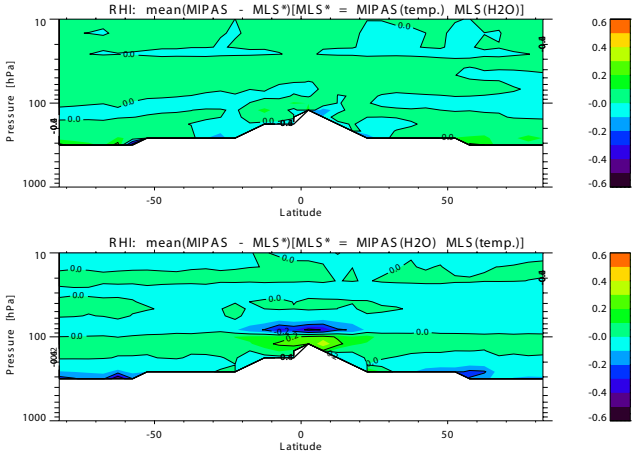

Fig. 12. Mean differences of MIPAS and MLS* RHI's (MIPAS-MLS*). Top panel: RHI is computed using MIPAS temperature and MLS H_2O profiles. Bottom panel: RHI is computed using MIPAS H_2O and MLS temperature profiles.

differences up to ∼5% (globally) between MLS and other instruments at the 21.5 hPa pressure level, which is also consistent with our comparison. However, we observe a positive difference of up to 20% at 31.6 hPa over the tropical region – a bias not appearing in the validation work by Froidevaux et al. (2008). The high relative differences over the tropics and sub-tropics in the TTL may partly be explained by low O_3 concentrations and strong vertical gradients in this region.

For ozone, Fig. 15 shows the global altitude-dependent mean bias together with the standard deviation and the error estimates. The bias profile lies within combined systematic error budget. A notch up to 0.26 ppmv (6.5%) is observed at 31.6 hPa exceeding the combined systematic error. The variability of the bias profiles is by up to a factor of four larger than the estimated noise error. Possible reasons are likely those which have already been discussed for temperature in Sect. 4.1.

4.5 HNO_3

Mean global distributions and comparisons of MIPAS and MLS HNO_3 are presented in Fig. 16. In the UTLS region (146.7–68.1 hPa) MIPAS and MLS are biased within 0.5–1 ppbv (up to 400%). In the lower to the middle stratosphere (68.1–14.6 hPa) differences are typically within 1 ppbv and relative differences up to 10–20%, with an exception over the tropics where at 31.6 hPa differences of 1 ppbv (about 400%) are observed.

In the UTLS region the positive difference observed in MIPAS versus MLS is in agreement with the low bias present in MLS (Santee et al., 2007). It had been reported by Santee et al. (2007) that MLS is uniformly low by 10–30% in the stratosphere. The MIPAS/MLS deviations reported here are in agreement with other comparisons reported by Santee et al. (2007) with the exception of the tropics around 31.6 hPa. Also Kinnison et al. (2008) have observed similar high relative differences in a comparison study between MLS and HIRDLS over the tropics. Since the structure appears like a second minimum over the tropics only in MLS and not in MIPAS distributions, it is attributed to an unexplained problem with MLS HNO_3 dataset.

The diagnosis plot of the global altitude-dependent mean bias is shown in Fig. 17. From 82.5 hPa to 6.8 hPa the

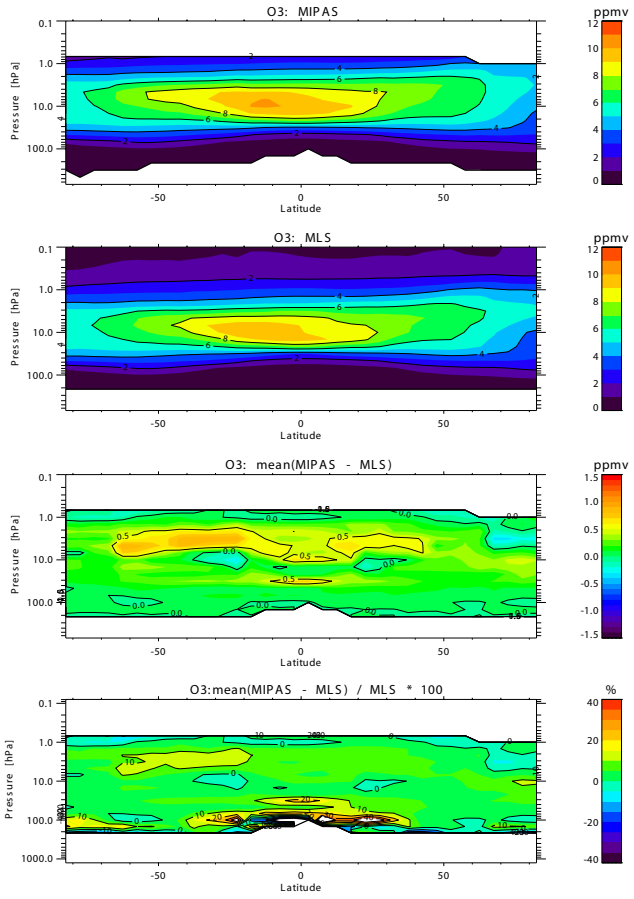

Fig. 13. Global O_3 field of MIPAS and MLS from 6 November to 7 December 2005 together with absolute and relative differences between MIPAS and MLS. The white patches at 100 hPa correspond to values beyond the colour scale.

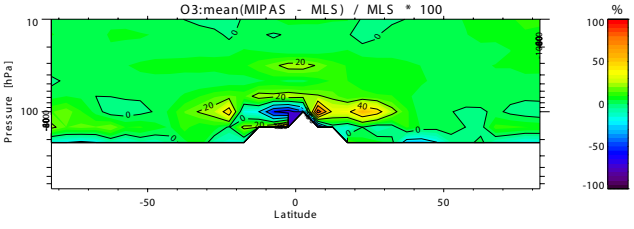

Fig. 14. Relative differences between MIPAS and MLS O_3 from 215 hPa–10 hPa.

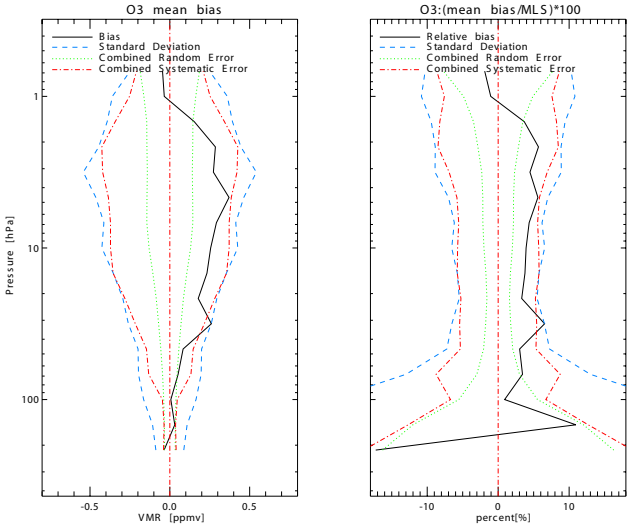

Fig. 15. Same as Fig. 10 but for O_3.

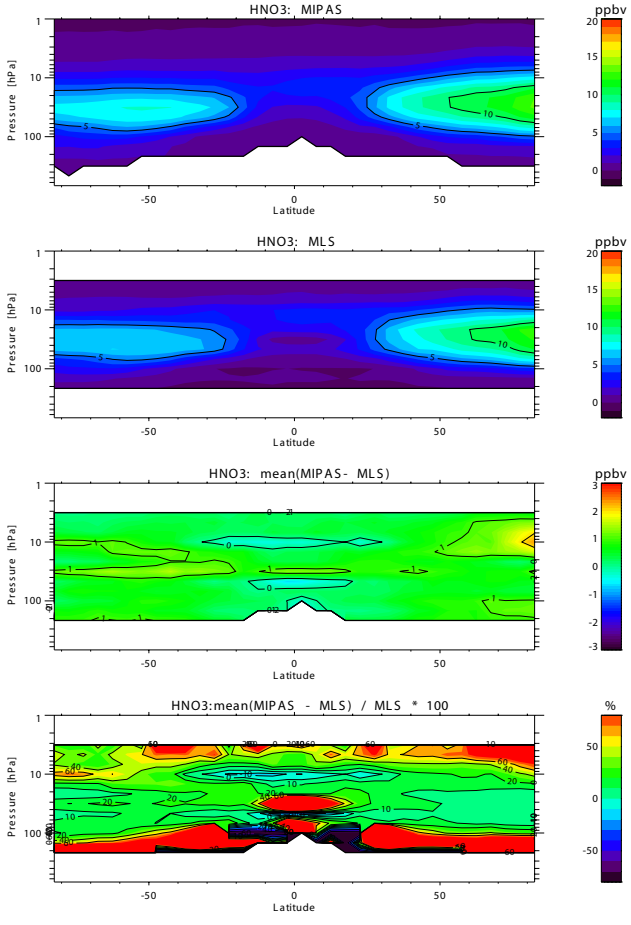

Fig. 16. Global HNO_3 field from MIPAS and MLS from 6 November to 7 December 2005. Mean absolute and relative differences between MIPAS and MLS. Colours beyond the colour scale (dark red and black) represent values outside the range of colour legend.

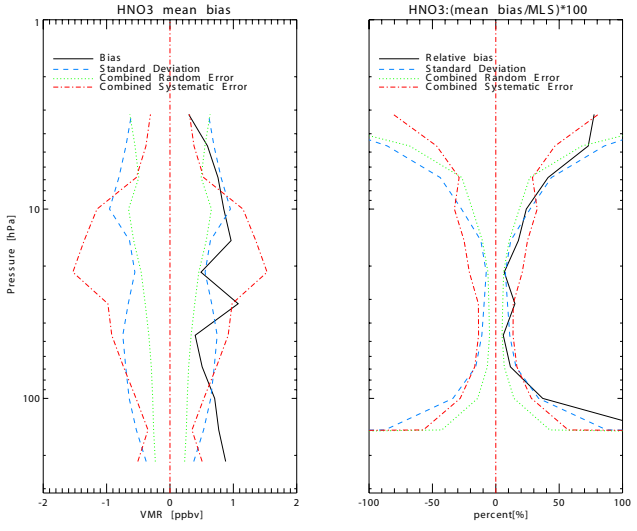

Fig. 17. Same as Fig. 10 but for HNO_3.

mean bias is well within the (1-σ) combined systematic errors, with the only exception at 31.6 hPa, as discussed above. Above 6.8 hPa and below 100 hPa the bias between the two instruments is slightly larger than estimated (by up to a factor of 2). The estimated noise is only slightly lower than the observed variability of the bias, and, thus more similar to the case of water vapour in the stratosphere than to temperature or ozone.

4.6 N_2O

The latitudinal distribution of N_2O vmr values of MIPAS and MLS and their related differences are shown in Fig. 18. In the lower stratosphere (100.0–21.5 hPa) MIPAS is typically up to 20% ($\leq$60 ppbv) larger than MLS along all latitudes. From 21.5 to 10.0 hPa agreement between MIPAS and MLS is typically about 5% (20 ppbv) in most of the latitude bins, apart from the subtropics and the north pole, where relative differences up to -10% and 20%, respectively, are observed. In the upper stratosphere (6.8–1.0 hPa) differences up to $\pm$10 ppbv and high relative differences are observed.

The positive bias of $\sim$10–15% in the lower stratosphere is attributed to the known positive bias in MIPAS retrievals (Payan et al., 2009; Glatthor et al., 2005). High relative differences observed in the upper stratosphere are due to low N_2O concentrations present in this region.

Figure 19 shows the globally averaged altitude-dependent mean bias between MIPAS and MLS together with its variation and estimated errors. The mean bias is well characterized within the combined systematic errors with minor exceptions below 68.1 hPa and at 4.6 hPa. Above about 10 hPa the combined estimated noise errors are similar to the standard deviation of the bias distributions. At lower altitudes the noise errors underestimate the variability, however,

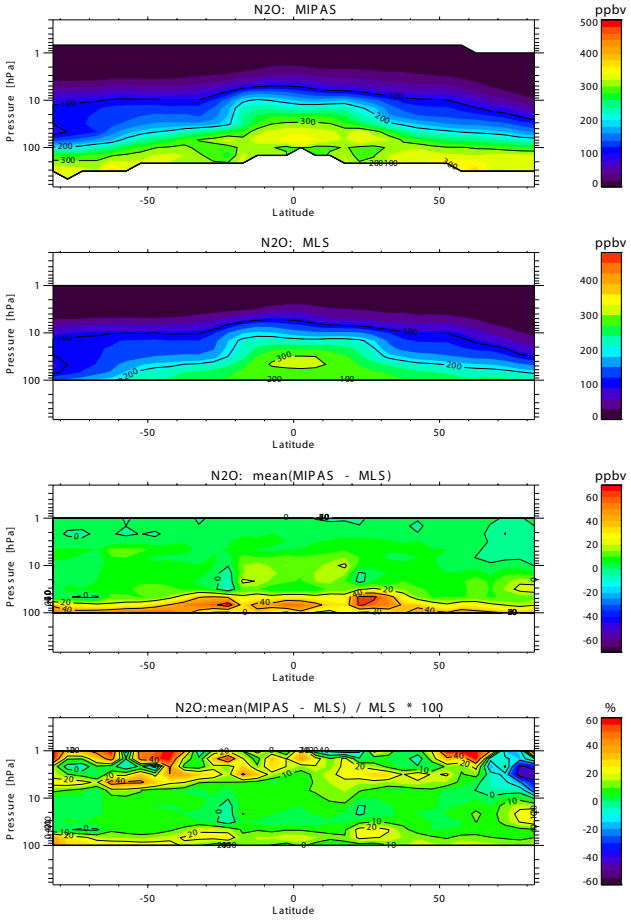

Fig. 18. Global N_2O field of MIPAS and MLS from 6 November to 7 December 2005 together with absolute and relative differences. Colours beyond the colour scale (dark red and black) represent values outside the range of colour legend.

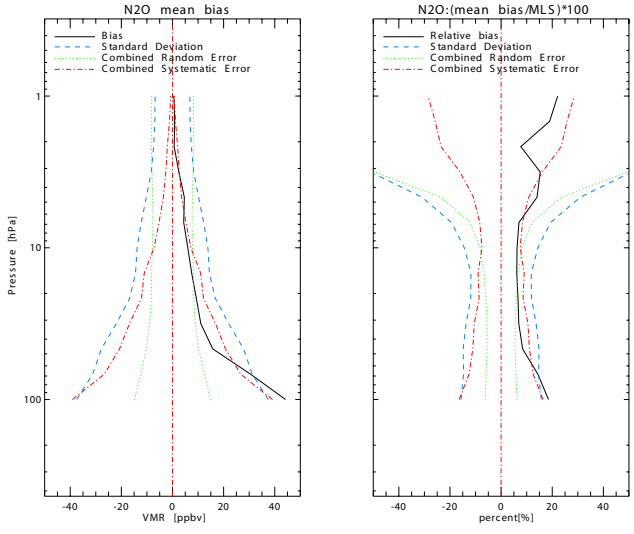

Fig. 19. Same as Fig. 10 but for N_2O.

as in case of stratospheric water vapour and HNO_3, only by up to a factor of about 2.

5 Conclusions

First IMK-IAA retrievals of temperature and trace gases from MIPAS reduced resolution (RR) UTLS-1 mode are shown. Vertical resolution and precision of RR UTLS-1 mode data are comparable to or better than MIPAS full resolution (FR) retrievals.

In contrast to the MIPAS FR observations, which have been performed before the launch of MLS, a comparison between the two limb-sounders was possible for the MIPAS UTLS-1 mode measurements of temperature, H_2O, relative humidity over ice, O_3, HNO_3 and N_2O. In general, the observed global mean altitude-dependent bias is well characterised by the estimated combined systematic errors of both instruments and no extreme outliers have been detected. Many of the observed discrepancies could be attributed to differences which have already been reported in previous validation studies and, thus, could be ascribed unambiguously to one of the instruments. Importantly, it has been shown that the new MIPAS IMK-IAA UTLS-1 mode dataset does not contain any significant deficiencies.

The variability of the global bias profiles cannot be explained by the estimated noise errors alone. We attribute this to a combination of atmospheric variability and parameter errors with distributions that may not be exactly specified.

Due to the similar altitude resolution and well characterized biases, the combination of MIPAS and MLS datasets seems possible. Since MIPAS trace gas observations at lower altitudes are in general more obstructed by clouds than those of MLS, synergistic use of MIPAS and MLS data can be useful e.g. in understanding H_2O/HNO_3 partitioning near tropical cirrus cloud and polar stratospheric cloud (PSC) studies. Further studies will indicate how far other species measured by both instruments provide a consistent picture of processes in the stratosphere and upper troposphere. If consistent, trace gases in the UTLS, such as CH_3CN which is observed by MLS, (although the reliability of the MLS v2.2 CH_3CN data has not yet been confirmed) and C_2H_2, C_2H_6 and PAN which are observed by MIPAS will then be used to complement each other for global pollution monitoring studies.

Similarly, in the stratosphere, both instruments together have the power to cover a large set of major inorganic chlorine and bromine species consistently: the chlorine species ClO (MLS, MIPAS), $ClONO_2$ (MIPAS) and HOCl (MIPAS, MLS), and HCl (MLS), or the bromine species BrO from MLS and, as discovered most recently, $BrONO_2$ from MIPAS (Höpfner et al., 2009), can be used to constrain halogen chemistry in models.

Acknowledgements. Re-processed MIPAS level-1B data were provided by ESA for scientific analysis. We gratefully acknowledge ECMWF for providing temperature field data and GES Distributed Active Archive Center for providing MLS temperature and trace gases data for comparison studies. This study has been funded by BMBF via contract no. 50 EE 0512 and by the EC project SCOUT-O3. The work at the Jet Propulsion Laboratory, California Institute of Technology was done under contract with NASA.

Edited by: H. Worden

References

Beer, R., Glavich, T. A., and Rider, D. M.: Tropospheric emission spectrometer for the Earth Observing System's Aura satellite, Appl. Optics, 40, 2356–2367, 2001.

Ceccherini, S., Cortesi, U., Verronen, P. T., and Kyrölä, E.: Technical Note: Continuity of MIPAS-ENVISAT operational ozone data quality from full- to reduced-spectral-resolution operation mode, Atmos. Chem. Phys., 8, 2201–2212, 2008, http://www.atmos-chem-phys.net/8/2201/2008/.

Echle, G., von Clarmann, T., Dudhia, A., Flaud, J.-M., Funke, B., Glatthor, N., Kerridge, B., López-Puertas, M., Martín-Torres, F. J., and Stiller, G. P.: Optimized spectral microwindows for data analysis of the Michelson Interferometer for Passive Atmospheric Sounding on the Environmental Satellite, Appl. Optics, 39, 5531–5540, 2000.

Eriksson, P., Ekström, M., Rydberg, B., and Murtagh, D. P.: First Odin sub-mm retrievals in the tropical upper troposphere: ice cloud properties, Atmos. Chem. Phys., 7, 471–483, 2007, http://www.atmos-chem-phys.net/7/471/2007/.

Fischer, H., Birk, M., Blom, C., Carli, B., Carlotti, M., von Clarmann, T., Delbouille, L., Dudhia, A., Ehhalt, D., Endemann, M., Flaud, J. M., Gessner, R., Kleinert, A., Koopman, R., Langen, J., López-Puertas, M., Mosner, P., Nett, H., Oelhaf, H., Perron, G., Remedios, J., Ridolfi, M., Stiller, G., and Zander, R.: MIPAS: an instrument for atmospheric and climate research, Atmos. Chem. Phys., 8, 2151–2188, 2008, http://www.atmos-chem-phys.net/8/2151/2008/.

Froidevaux, L., Jiang, Y., Lambert, A., Livesey, N., Read, W., Waters, J., Browell, E., Hair, J., Avery, M., McGee, T., Twigg, L., Sumnicht, G., Jucks, K., Margitan, J., Sen, B., Stachnik, R., Toon, G., Bernath, P., Boone, C., Walker, K., Filipiak, M., Harwood, R., Fuller, R., Manney, G., Schwartz, M., Daffer, W., Drouin, B., Cofield, R., Cuddy, D., Jarnot, R., Knosp, B., Perun, V., Snyder, W., Stek, P., Thurstans, R., and Wagner, P.: Validation of Aura Microwave Limb Sounder stratospheric ozone measurements, J. Geophys. Res., 113, D15S20, doi:10.1029/2007JD008771, 2008.

Gille, J., Barnett, J., Arter, P., Barker, M., Bernath, P., Boone, C., Cavanaugh, C., Chow, J., Coffey, M., Craft, J., Craig, C., Dials, M., Dean, V., Eden, T., Edwards, D., Francis, G., Halvorson, C., Harvey, L., Hepplewhite, C., Khosravi, R., Kinnison, D., Krinsky, C., Lambert, A., Lee, H., Lyjak, L., Loh, J., Mankin, W., Massie, S., McInerney, J., Moorhous, J., Nardi, B., Packman, D., Randall, C., Reburn, J., Rudolf, W., Schwartz, M., Serafin, J., Stone, K., Torpy, B., Walker, K., Waterfall, A., Watkins, R., Whitney, J., Woodard, D., and Young, G.: The High Resolution Dynamics Limb Sounder (HIRDLS): Experiment Overview, Recovery and Validation of Initial Temperature Data, J. Geophys. Res., 113, D16S43, doi:10.1029/2007JD008824, 2008.

Glatthor, N., von Clarmann, T., Fischer, H., Funke, B., Grabowski, U., Höpfner, M., Kellmann, S., Kiefer, M., Linden, A., Milz, M., Steck, T., Stiller, G. P., Mengistu Tsidu, G., and Wang, D. Y.: Mixing processes during the Antarctic vortex split in September/October 2002 as inferred from source gas and ozone distributions from ENVISAT-MIPAS, J. Atmos. Sci., 62, 787–800, 2005.

Glatthor, N., von Clarmann, T., Fischer, H., Funke, B., Grabowski, U., Höpfner, M., Kellmann, S., Kiefer, M., Linden, A., Milz, M., Steck, T., and Stiller, G. P.: Global peroxyacetyl nitrate (PAN) retrieval in the upper troposphere from limb emission spectra of the Michelson Interferometer for Passive Atmospheric Sounding (MIPAS), Atmos. Chem. Phys., 7, 2775–2787, 2007, http://www.atmos-chem-phys.net/7/2775/2007/.

Goff, J. A. and Gratch, S.: Low-pressure properties of water from −160 to 212 F, in Transactions of the American society of heating and ventilating engineers presented at the 52nd annual meeting of the American society of heating and ventilating engineers New York, 95–122, 1946.

Höpfner, M., Orphal, J., von Clarmann, T., Stiller, G., and Fischer, H.: Stratospheric $BrONO_2$ observed by MIPAS, Atmos. Chem. Phys., 9, 1735–1746, 2009, http://www.atmos-chem-phys.net/9/1735/2009/.

Jiang, J. H., Livesey, N. J., Su, H., Neary, L., McConnell, J. C., and Richards, N. A. D.: Connecting surface emissions, conrective uplifting and long-range transport of carbon monoxide in the upper troposphere: New observations from the Aura Microwave Limb Sounder, Geophys. Res. Lett., 34, L18812, doi:10.1029/2007GL030638, 2007.

Kinnison, D., Gille, J., Barnett, J., Randall, C., Harvey, V., Lambert, A., Khosravi, R., Alexander, M., Bernath, P., Boone, C., Cavanaugh, C., Coffey, M., Craig, C., Dean, V., Eden, T., Ellis, D., Fahey, D., Francis, G., Halvorson, C., Hannigan, J., Hartsough, C., Hepplewhite, C., Krinsky, C., Lee, H., Mankin, W., Marcy, T., Massie, S., Nardi, B., Packman, D., Popp, P., Santee, M., Yudin, V., and Walker, K.: Global Observations of HNO_3 from the High Resolution Dynamics Limb Sounder (HIRDLS) – First results, J. Geophys. Res., 113, D16S44, doi:10.1029/2007JD008814, 2008.

Lambert, A., Read, W., Livesey, N., Santee, M., Manney, G., Froidevaux, L., Wu, D., Schwartz, M., Pumphrey, H., Jimenez, C., Nedoluha, G., Cofield, R., Cuddy, D., Daffer, W., Drouin, B., Fuller, R., Jarnot, R., Knosp, B., Pickett, H., Perun, V., Snyder, W., Stek, P., Thurstans, R., Wagner, P., Waters, J., Jucks, K., Toon, G., Stachnik, R., Bernath, P., Boone, C., Walker, K., Urban, J., Murtagh, D., Elkins, J., and Atlas, E.: Validation of the Aura Microwave Limb Sounder middle atmosphere water vapor and nitrous oxide measurements, J. Geophys. Res., 112, D24S36, doi:10.1029/2007JD008724, 2007.

Livesey, N., Snyder, W., Read, W., and Wagner, P.: Retrieval algorithms for the EOS Microwave Limb Sounder (MLS) instrument, IEEE T. Geosci. Remote, 44, 1144–1155, 2006.

Livesey, N. J., Filipak, M. J., Froidevaux, L., Read, W. G., Lambert, A., Santee, M. L., Jiang, J. H., Pumphrey, H. C., Waters, J. W., Cofield, R. E., Cuddy, D. T., Daffer, W. H., Drouin, B. J., Fuller, R. A., Jarnot, R. F., Jiang, Y. B., Knosp, B. W., Li, Q. B., Perun, V. S., Schwartz, M. J., Snyder, W. V., Stek, P. C.,

Thurstans, R. P., Wagner, P. A., Avery, M., Browell, E. V., Cammas, J.-P., Christensen, L. E., Diskin, G. S., Gao, R.-S., Jost, H.-J., Loewenstein, M., Lopez, J. D., Nedelec, P., Osterman, G. B., Sachse, G. W., and Webster, C. R.: Validation of Aura Microwave Limb Sounder O_3 and CO observations in the upper troposphere and lower stratosphere, J. Geophys. Res., 113, D15S02, doi:10.1029/2007JD008805, 2008.

Milz, M., von Clarmann, T., Fischer, H., Glatthor, N., Grabowski, U., Höpfner, M., Kellmann, S., Kiefer, M., Linden, A., Mengistu Tsidu, G., Steck, T., Stiller, G. P., Funke, B., López-Puertas, M., and Koukouli, M. E.: Water Vapor Distributions Measured with the Michelson Interferometer for Passive Atmospheric Sounding on board Envisat (MIPAS/Envisat), J. Geophys. Res., 110, D24307, doi:10.1029/2005JD005973, 2005.

Murtagh, D., Frisk, U., Merino, F., Ridal, M., Jonsson, A., Stegman, J., Witt, G., Eriksson, P., Jiménez, C., Megie, G., de la Nöe, J., Ricaud, P., Baron, P., Pardo, J. R., Hauchcorne, A., Llewellyn, E. J., Degenstein, D. A., Gattinger, R. L., Lloyd, N. D., Evans, W. F. J., McDade, I. C., Haley, C. S., Sioris, C., von Savigny, C., Solheim, B. H., McConnell, J. C., Strong, K., Richardson, E. H., Leppelmeier, G. W., Kyrölä, E., Auvinen, H., and Oikarinen, L.: An overview of the Odin atmospheric mission, Can. J. Phys., 80, 309–319, doi:10.1139/P01-157, 2002.

Payan, S., Camy-Peyret, C., Oelhaf, H., Wetzel, G., Maucher, G., Keim, C., Pirre, M., Huret, N., Engel, A., Volk, M. C., Kuellmann, H., Kuttippurath, J., Cortesi, U., Bianchini, G., Mencaraglia, F., Raspollini, P., Redaelli, G., Vigouroux, C., De Mazière, M., Mikuteit, S., Blumenstock, T., Velazco, V., Notholt, J., Mahieu, E., Duchatelet, P., Smale, D., Wood, S., Jones, N., Piccolo, C., Payne, V., Bracher, A., Glatthor, N., Stiller, G., Grunow, K., Jeseck, P., Te, Y., and Butz, A.: Validation of version-4.61 methane and nitrous oxide observed by MIPAS, Atmos. Chem. Phys., 9, 413–442, 2009, http://www.atmos-chem-phys.net/9/413/2009/.

Read, W., Lambert, A., Bacmeister, J., Cofield, R., Christensen, L., Cuddy, D., Daffer, W., Drouin, B., Fetzer, E., Froidevaux, L., Fuller, R., Herman, R., Jarnot, R., Jiang, J., Jiang, Y., Kelly, K., Knosp, B., Pumphrey, H., Rosenlof, K., Sabounchi, X., Santee, M., Schwartz, M., Snyder, W., Stek, P., Su, H., Takacs, L., Thurstans, R., Vomel, H., Wagner, P., Waters, J., Webster, C., Weinstock, E., and Wu, D.: Aura Microwave Limb Sounder upper tropospheric and lower stratospheric H_2O and relative humidity with respect on ice validation, J. Geophys. Res. 112, D24S35, doi:10.1029/2007JD008752, 2007.

Read, W. G., Waters, J. W., Froidevaux, L., Flower, D. A., Jarnot, R. F., Hartmann, D. L., Harwood, R. S., and Rood, R. B.: Upper-tropospheric water vapor from UARS MLS, B. Am. Meteorol. Soc., 76, 2381–2389, 1995.

Read, W. G., Wu, D. L., Waters, J. W., and Pumphrey, H. C.: Dehydration in the tropical tropopause layer: Implications from the UARS Microwave Limb Sounder, J. Geophys. Res., 109, D06110, doi:10.1029/2003JD004056, 2004.

Rodgers, C. D.: Inverse Methods for Atmospheric Sounding: Theory and Practice, in: Series on Atmospheric, Oceanic and Planetary Physics, edited by: Taylor, F. W., World Scientific, 2, 2000.

Santee, M., Lambert, A., Read, W., Livesey, N., Cofield, R., Cuddy, D., Daffer, W., Drouin, B., Froidevaux, L., Fuller, R., Jarnot, R., Knosp, B., Manney, G., Perun, V., Snyder, W., Stek, P., Thurstans, R., Wagner, P., Waters, J., Muscari, G., deZafra, R., Dibb, J., Fahey, D., Popp, P., Marcy, T., Jucks, K., Toon, G., Stachnik, R., Bernath, P., Boone, C., Walker, K., Urban, J., and Murtagh, D.: Validation of Aura Microwave Limb Sounder HNO_3 Measurements, J. Geophys. Res., 112, D24S40, doi:10.1029/2007JD008721, 2007.

Schoeberl, M., Douglass, A., Hilsenrath, E., Bhartia, P., Barnett, J., Beer, R., Waters, J., Gunson, M., Froidevaux, L., Gille, J., Levelt, P., and DeCola, P.: Overview of the EOS Aura Mission, IEEE T. Geosci. Remote, 44, 1066–1074, 2006.

Schwartz, M., Lambert, A., Manney, G., Read, W., Livesey, N., Froidevaux, L., Ao, C., Bernath, P., Boone, C., Cofield, R., Daffer, W., Drouin, B., Fetzer, E., Fuller, R., Jarnot, R., Jiang, J., Jiang, Y., Knosp, B., Kruger, K., Li, J.-L., Mlynczak, M., Pawson III, S., Russell III, J. M., Santee, M., Snyder, W., Stek, P., Thurstans, R., Tompkins, A., Wagner, P., Walker, K., Waters, J., and Wu, D.: Validation of the Aura Microwave Limb Sounder Temperature and Geopotential Height Measurements, J. Geophys. Res., 113, D15S11, doi:10.1029/2007JD008783, 2008.

Spang, R., Remedios, J. J., and Barkley, M. P.: Colour indices for the detection and differentiation of cloud types in infra-red limb emission spectra, Adv. Space Res., 3, 1041–1047, doi:10.1016/S0273-1177(03)00585-4, 2004.

Steck, T.: Bestimmung von Vertikalprofilen von Spurengasen aus MIPAS-Messungen unter Hinzunahme von a priori Wissen, Ph.D. thesis, Institut für Meteorologie und Klimaforschung, Universität Karlsruhe, Kernforschungszentrum Karlsruhe, dissertation, DLR-FB 2000-01, ISSN 1434-8454, 2000.

Steck, T.: Methods for determining regularization for atmospheric retrieval problems, Appl. Optics, 41, 1788–1797, 2002.

Steck, T. and von Clarmann, T.: Constrained profile retrieval applied to the observation mode of the Michelson Interferometer for Passive Atmospheric Sounding, Appl. Optics, 40, 3559–3571, 2001.

Steck, T., von Clarmann, T., Fischer, H., Funke, B., Glatthor, N., Grabowski, U., Höpfner, M., Kellmann, S., Kiefer, M., Linden, A., Milz, M., Stiller, G. P., Wang, D. Y., Allaart, M., Blumenstock, Th., von der Gathen, P., Hansen, G., Hase, F., Hochschild, G., Kopp, G., Kyrö, E., Oelhaf, H., Raffalski, U., Redondas Marrero, A., Remsberg, E., Russell III, J., Stebel, K., Steinbrecht, W., Wetzel, G., Yela, M., and Zhang, G.: Bias determination and precision validation of ozone profiles from MIPAS-Envisat retrieved with the IMK-IAA processor, Atmos. Chem. Phys., 7, 3639–3662, 2007, http://www.atmos-chem-phys.net/7/3639/2007/.

Su, H., Read, W. G., Jiang, J. H., Waters, J. W., Wu, D. L., and Fetzer, E. J.: Enhanced positive water vapor feedback associated with tropical deep convection: New evidence from Aura MLS, Geophys. Res. Lett., 33, L05709, doi:10.1029/2005GL025505, 2006.

Tikhonov, A.: On the solution of incorrectly stated problems and method of regularization, Dokl. Akad. Nauk SSSR+, 151, 501–504, 1963.

von Clarmann, T.: Validation of remotely sensed profiles of atmospheric state variables: strategies and terminology, Atmos. Chem. Phys., 6, 4311–4320, 2006, http://www.atmos-chem-phys.net/6/4311/2006/.

von Clarmann, T., Glatthor, N., Grabowski, U., Höpfner, M., Kellmann, S., Kiefer, M., Linden, A., Mengistu Tsidu, G., Milz, M., Steck, T., Stiller, G. P., Wang, D. Y., Fischer, H., Funke, B., Gil-López, S., and López-Puertas, M.: Retrieval of temper-

ature and tangent altitude pointing from limb emission spectra recorded from space by the Michelson Interferometer for Passive Atmospheric Sounding (MIPAS), J. Geophys. Res., 108, 4736, doi:10.1029/2003JD003602, 2003.

von Clarmann, T., Glatthor, N., Koukouli, M. E., Stiller, G. P., Funke, B., Grabowski, U., Höpfner, M., Kellmann, S., Linden, A., Milz, M., Steck, T., and Fischer, H.: MIPAS measurements of upper tropospheric $C-2H_6$ and O_3 during the southern hemispheric biomass burning season in 2003, Atmos. Chem. Phys., 7, 5861–5872, 2007, http://www.atmos-chem-phys.net/7/5861/2007/.

von Clarmann, T., De Clercq, C., Ridolfi, M., Höpfner, M., and Lambert, J.-C.: The horizontal resolution of MIPAS, Atmos. Meas. Techn. Discuss., 1, 103–125, 2008.

von Clarmann, T., De Clercq, C., Ridolfi, M., Höpfner, M., and Lambert, J.-C.: The horizontal resolution of MIPAS, Atmos. Meas. Techn., 2, 47–54, 2009a.

von Clarmann, T., Höpfner, M., Kellmann, S., Linden, A., Chauhan, S., Funke, B., Grabowski, U., Glatthor, N., Kiefer, M., Schieferdecker, T., Stiller, G. P., and Versick, S.: Retrieval of temperature, H_2O, O_3, HNO_3, CH_4, N_2O, $ClONO_2$ and ClO from MIPAS reduced resolution nominal mode limb emission measurements, Atmos. Meas. Tech., 2, 159–175, 2009b.

Wang, D. Y., von Clarmann, T., Fischer, H., Funke, B., Gil-López, S., Glatthor, N., Grabowski, U., Höpfner, M., Kaufmann, M., Kellmann, S., Kiefer, M., Koukouli, M. E., Linden, A., López-Puertas, M., Mengistu Tsidu, G., Milz, M., Steck, T., Stiller, G. P., Simmons, A. J., Dethof, A., Swinbank, R., Marquardt, C., Jiang, J. H., Romans, L. J., Wickert, J., Schmidt, T., Russell III, J., and Remsberg, E.: Validation of stratospheric temperatures measured by Michelson Interferometer for Passive Atmospheric Sounding MIPAS on Envisat, J. Geophys. Res., 110, D08301, doi:10.1029/2004JD005342, 2005.

Wang, D. Y., Höpfner, M., Mengistu Tsidu, G., Stiller, G. P., von Clarmann, T., Fischer, H., Blumenstock, T., Glatthor, N., Grabowski, U., Hase, F., Kellmann, S., Linden, A., Milz, M., Oelhaf, H., Schneider, M., Steck, T., Wetzel, G., López-Puertas, M., Funke, B., Koukouli, M. E., Nakajima, H., Sugita, T., Irie, H., Urban, J., Murtagh, D., Santee, M. L., Toon, G., Gunson, M. R., Irion, F. W., Boone, C. D., Walker, K., and Bernath, P. F.: Validation of nitric acid retrieved by the IMK-IAA processor from MIPAS/ENVISAT measurements, Atmos. Chem. Phys., 7, 721–738, 2007, http://www.atmos-chem-phys.net/7/721/2007/.

Waters, J., Froidevaux, L., Harwood, R., Jarnot, R., Pickett, H., Read, W., Siegel, P., Cofield, R., Filipiak, M., Flower, D., Holden, J., Lau, G., Livesey, N., Manney, G., Pumphrey, H., Santee, M., Wu, D., Cuddy, D., Lay, R., Loo, M., Perun, V., Schwartz, M., Stek, P., Thurstans, R., Boyles, M., Chandra, S., Chavez, M., Chen, G.-S., Chudasama, B., Dodge, R., Fuller, R., Girard, M., Jiang, J., Jiang, Y., Knosp, B., LaBelle, R., Lee, K., Miller, D., Oswald, J., Patel, N., Pukala, D., Quintero, O., Scaff, D., Snyder, W., Tope, M., Wagner, P., and Walch, M.: The Earth Observing System Microwave Limb Sounder (EOS MLS) on the Aura satellite, IEEE T. Geosci. Remote, 44(5), 1075–1092, 2006.

Wu, D., Read, W., Dessler, A., Sherwood, S., and Jiang, J.: UARS MLS Cloud Ice Measurements and Implications for H_2O Transport near the Tropopause, Journal of Atmospheric Sciences, 62, 518–530, 2005.